

Stationary shear flows of dense granular materials : a tentative continuum modelling

C. Josserand, P.-Y. Lagrée and D. Lhuillier
Laboratoire de Modélisation en Mécanique,
Université P. et M. Curie (Paris 6) et CNRS
Case 162, 4 place Jussieu, 75252 Paris cedex 05, France

January 13, 2004

Abstract

We propose a simple continuum model to interpret the shearing motion of dense, dry and cohesion-less granular media. Compressibility, dilatancy and Coulomb-like friction are the three basic ingredients. The granular stress is split into a rate-dependent part representing the rebound-less impacts between grains and a rate-independent part associated with long-lived contacts. Because we consider stationary flows only, the grain compaction and the grain velocity are the two main variables. The predicted velocity and compaction profiles are in apparent agreement with the experimental or numerical results concerning free-surface shear flows as well as confined shear flows

1 Introduction

The mechanical behaviour of a flowing granular material depends strongly on the grain compaction. While dense granular media usually exhibit relatively slow motions with predominance of friction, less dense ones are usually found in vigorous motions with predominance of two-particles collisions. The collision-dominated regime is well described by kinetic theory, with the concepts of granular temperature and inelastic collisions. On the contrary, the current description of dense granular flows is not so fully satisfactory. It must be understood that we are not questioning the description by soil mechanics of quasi-static and highly stressed granular materials, but the description of flows with relatively low stress levels encountered, for example, in avalanches

down an inclined plane. Several recent works (see e.g. [1, 2, 3]) concluded rather pessimistically about the possibility of describing dense granular flows within the realm of continuum mechanics. In fact, the experimental observation that most dense flows display a typical thickness of a few grain diameters must not be a factor of pessimism. We know from several examples in suspension mechanics that the continuum approach can cope with high velocity gradients in one direction, provided one has some statistical homogeneity in the other two directions. This situation is exactly the one met in sheared granular media, provided we discard transient effects and focus on the final stationary state. Once the continuum description is accepted, the number of relevant field variables must be decided. There is no doubt that the grain velocity is relevant and it is not less clear that the grain compaction is also a pertinent variable. In fact the widely used assumption of an incompressible medium is not tenable. It contradicts the dilatancy concept and, as will be seen below, the transport coefficients of a dense granular medium display enormous variations with only tiny modifications of the compaction. Our aim is thus to propose a model for dense and stationary shear flows in which the grain compaction and the grain velocity are the two fundamental variables. One could also suggest the fluctuational kinetic energy of the grains (the granular "temperature") as a third variable. However, since we limit our analysis to stationary shears, the granular temperature is no longer an independent variable. The role of the embedding fluid will be neglected everywhere, and for these "dry" granular media, the main issue is to propose a constitutive relation for the granular stress. To compare with previous works on dense flows, we can say we adopt a phenomenological description somewhat similar to that proposed two decades ago by Savage [4] and by Johnson and Jackson [5]. Like these authors, we introduce a stress tensor split into a frictional and a collisional contribution. However, the collisional contribution is concerned with rebound-less impacts characteristic of high grain concentration, and is free of any restitution coefficient. Our constitutive relation for the particulate stress has a form somewhat similar to that proposed by Ancey and Evesque [6], the main differences concerning the role of the grain compaction and a more detailed expression of the granular pressure. Our model also shares some common features with the model proposed by Bocquet et al. [7] and by Louge [8], but instead of extending the kinetic theory approach to large compaction, we prefer here to develop a model specifically devoted to dense media. Moreover, the model we propose is quite simple in so far as it denies any special role to the compaction gradient [9] and avoids the non-locality concept [10].

Discarding two-particles collisions and any restitution coefficient means that our model is restricted to volume fractions in the range between ϕ_m

and ϕ_M . The maximum grain compaction ϕ_M corresponds to the highest possible random packing (with $\phi_M \simeq 0.80$ for two-dimensional flows and $\phi_M \simeq 0.65$ for three-dimensional ones) while ϕ_m is the smallest compaction compatible with the existence of a continuous network of contacts between grains. As suggested by Azanza [1], one can define ϕ_m as the minimum compaction for which the two-particle distribution function exhibits some swelling at a distance of *two* diameters. With this definition, $\phi_m \simeq 0.70$ for two-dimensional flows while $\phi_m \simeq 0.50$ for three-dimensional ones.

A phenomenological order parameter description of granular media was recently proposed [11]. We acknowledge this approach looks efficient in describing a large number of phenomena observed in dense flows, but it suffers from two serious drawbacks. The first one is the huge number of possible candidates for the order parameter. For example, in the model to be presented below, the reduced compaction $(\phi - \phi_m)/(\phi_M - \phi_m)$ could play this role. A second difficulty concerns the relevance of the Ginzburg-Landau relaxation equation for the order parameter. Here we consider the standard conservation of mass and momentum only, without any extra equation.

The description of stationary free-surface shear flows is given in section 2 while that of confined shear flows is presented in section 3. Section 4 compares the model predictions with experimental and (or) numerical data. The final section insists on the limitations and necessary improvements of the proposed model, which must be considered as a minimal one.

2 Free surface shear-flows

As a prototype of shear flow with free surface, we consider the gravity-induced chute (over a heap or an inclined plate, see Figure 1) with an angle θ relative to the horizontal plane. The mean grain velocity is parallel to the x -axis, $\mathbf{V} = V\mathbf{e}_x$, while V and the solid fraction ϕ depend only on z , the *distance to the free surface*. The granular stress tensor is noted τ and the equations of motion are:

$$0 = -\frac{\partial\tau_{xz}}{\partial z} + \phi\rho g\sin(\theta), \quad 0 = -\frac{\partial\tau_{zz}}{\partial z} + \phi\rho g\cos(\theta) \quad (1)$$

where ρ is the constant mass per unit volume of the grain material and g is the acceleration of gravity.

For dense granular media, the granular stress is a consequence of long-lived contacts and bounce-less impacts between grains. Long-lived contacts result from compressive forces acting towards the boundaries of the granular medium. In the geometry considered, they take part in τ_{zz} since z is

the direction of main compression. Whether gravity is responsible for compressive forces or not, we choose to scale the compressive stress with $\rho g D$ where D is the grain size. The compressive stresses are related to the grain volume fraction as $\rho g D F(\phi)$, where $dF/d\phi$ is the non-dimensional compressibility of the granular medium. In free-surface shear flows, gravity is the only source of compaction and the magnitude of the compressive stress will also depend on θ . It is clear that the compressive role of gravity is maximum when the compression axis z is vertical while this role vanishes when gravity is orthogonal to it. Consequently, the general form of the gravity-induced compressive stress is $\rho g D F(\phi) f(\theta)$ with $f(0) = 1$ and $f(\pi/2) = 0$. The exact expression of $f(\theta)$ is not important because, as will soon be seen, the stationary flows exist in a very limited range of θ only. One of the simplest function of θ which meets the above requirement is $\cos(\theta)$, and we assume henceforth that the contribution of long-lived contacts to τ_{zz} can be written in the form $\rho g D F(\phi) \cos(\theta)$. To this gravity-induced contact stress must be added a rate-dependent impact stress. On purely dimensional grounds, this second contribution cannot be but Bagnold-like and the full normal stress finally appears in the form:

$$\tau_{zz} = \rho D^2 \mu_N(\phi) \left(\frac{dV}{dz} \right)^2 + \rho g D F(\phi) \cos(\theta), \quad (2)$$

where $\mu_N(\phi)$ represents the compaction-dependent intensity of the normal stress induced by the shear rate. Concerning the shear stress of the flowing granular medium, we assume it is made of a Coulomb-like contribution with a friction coefficient $\mu(\phi)$ completed by a Bagnold-like contribution involving a coefficient $\mu_T(\phi)$ representing the compaction-dependent intensity of the shear stress induced by the shear rate

$$\tau_{xz} = \rho D^2 \mu_T(\phi) \left(\frac{dV}{dz} \right)^2 + \mu(\phi) \tau_{zz}, \quad (3)$$

The model expressions (2) and (3) contain four functions of the grain compaction. Before giving them some explicit (and tentative) expressions, let us comment on their expected general behaviour. These four functions are characteristic of the dense regime and have a meaning in the range $\phi_m \leq \phi \leq \phi_M$ only. We expect F , μ_T and μ_N to become infinite when $\phi = \phi_M$, because no motion nor extra compaction is expected above the maximum random packing. We also expect F and μ_N to vanish for $\phi = \phi_m$, because the normal stresses must vanish for the most tenuous contact network. Concerning the friction coefficient μ , it is the only coefficient which remains finite when $\phi = \phi_M$ and it presumably increases [12] for smaller compactions. In short,

the three scalars F , μ_N and μ_T are strongly increasing functions of the compaction, while μ has a much smoother behaviour.

Since we neglect the role of the embedding fluid, the granular stress must vanish at the free surface and consequently $\tau_{xz} = \tan(\theta)\tau_{zz}$ everywhere. In this case, when solving the equations of motion (1) with the model expressions (2) and (3), one arrives at a compaction profile and a velocity profile which are solution of:

$$D \frac{d\phi}{dz} = \frac{\phi}{\frac{\partial}{\partial \phi} \left[\frac{F}{1 - (\mu_N/\mu_T)(\tan(\theta) - \mu)} \right]} \quad (4)$$

and

$$\left(\frac{D}{g} \right)^{1/2} \frac{dV}{dz} = - \left(\frac{F(\sin(\theta) - \mu \cos(\theta))}{\mu_T(1 - (\mu_N/\mu_T)(\tan(\theta) - \mu))} \right)^{1/2}. \quad (5)$$

At the free-surface the solid fraction is ϕ_m (remember we limit the description to the dense regime). According to (4) the solid fraction increases towards its maximum value ϕ_M over a depth which scales with the grain diameter but depends on θ if μ_N/μ_T is different from zero. Hence μ_N/μ_T represents the relative magnitude of Reynold's dilatancy. Concerning the velocity profile, its characteristic value scales like $(gD)^{1/2}$ and according to (5) its solution exists for any angle θ verifying the inequality $\mu(\phi) \leq \tan(\theta) \leq \mu(\phi) + \mu_T(\phi)/\mu_N(\phi)$. For certain values of θ this inequality is possibly satisfied in a part only of the full range $\phi_m \leq \phi \leq \phi_M$.

It is obviously not evident to deduce four functions of the compaction from the rather scarce experimental or numerical results on stationary shear flows. *We assume henceforth that μ and μ_T/μ_N are independent of the grain compaction.* Then, a stationary solution is possible in a well-defined angle range $\theta_{min} \leq \theta \leq \theta_{max}$, with $\tan(\theta_{min}) = \mu$ and $\tan(\theta_{max}) = \mu + \mu_T/\mu_N$. To obtain more quantitative results we consider separately the chute over a heap from that over an inclined plane.

2.1 Heap flows

In the heap case, provided μ and μ_N/μ_T are independant of the solid fraction, one can deduce from (4) and (5) the total granular flux flowing down the heap Q_{heap} :

$$\frac{Q_{heap}}{D\sqrt{gD}} = \frac{(\sin(\theta) - \mu \cos(\theta))^{1/2}}{\left(1 - \frac{\mu_N}{\mu_T}(\tan(\theta) - \mu)\right)^{5/2}} \int_{\phi_m}^{\phi_M} \left(\frac{F^3}{\mu_T}\right)^{1/2} \frac{\partial F}{\partial \phi} \frac{d\phi}{\phi} \quad (6)$$

the grain velocity $V_{heap}(0)$ at the free surface

$$\frac{V_{heap}(0)}{\sqrt{gD}} = \frac{(\sin(\theta) - \mu \cos(\theta))^{1/2}}{\left(1 - \frac{\mu_N}{\mu_T}(\tan(\theta) - \mu)\right)^{3/2}} \int_{\phi_m}^{\phi_M} \left(\frac{F}{\mu_T}\right)^{1/2} \frac{\partial F}{\partial \phi} \frac{d\phi}{\phi} \quad (7)$$

and the relative velocity profile

$$\frac{V_{heap}(z)}{V_{heap}(0)} = \frac{\int_{\phi_{heap}(z)}^{\phi_M} \left(\frac{F}{\mu_T}\right)^{1/2} \frac{\partial F}{\partial \phi} \frac{d\phi}{\phi}}{\int_{\phi_m}^{\phi_M} \left(\frac{F}{\mu_T}\right)^{1/2} \frac{\partial F}{\partial \phi} \frac{d\phi}{\phi}} \quad (8)$$

Since the free-surface velocity and the flux are expected to have finite values for $\theta_{min} < \theta < \theta_{max}$, the two functions $F(\phi)$ and $\mu_T(\phi)$ must be such as to guarantee the convergence of the above integrals. In this case $V_{heap}(0)$ and Q_{heap} are function of θ with numerical prefactors depending on one's peculiar choice for F and μ_T . In what follows we adopt the simple expressions

$$F = F_0 \text{Log} \left(\frac{\phi_M - \phi_m}{\phi_M - \phi} \right) \quad \text{and} \quad \mu_T = \mu_{T0} \left(\frac{\phi_M - \phi_m}{\phi_M - \phi} \right)^2. \quad (9)$$

The same expression for F was already proposed by Savage [4, 13] and leads to an exponential-like volume fraction profile:

$$\phi_{heap}(z, \theta) = \frac{\phi_M}{1 + \left(\frac{\phi_M}{\phi_m} - 1\right)e^{-z/L(\theta)}} \quad (10)$$

with

$$L(\theta) = \frac{F_0 D}{\phi_M \left(1 - \frac{\mu_N}{\mu_T}(\tan(\theta) - \mu)\right)} \quad (11)$$

$L(\theta)$ represents the typical thickness of the layer flowing down the heap, and it increases from $L(\theta_{min}) = \frac{F_0 D}{\phi_M}$ to infinity when $\theta = \theta_{max}$. The relative velocity profile is also exponential-like for $\frac{z}{L(\theta)} \gtrsim 2$ (see figure 2) but displays a Bagnold-like region of inverse concavity for $\frac{z}{L(\theta)} \lesssim 0.2$ (see figure 3). In fact, the numerical solution can be fitted by the analytical expression

$$1 - \frac{V_{heap}(z)}{V_{heap}(0)} = \left(\frac{\phi_{heap}(z) - \phi_m}{\phi_M - \phi_m} \right)^{\frac{3}{2}} = \left(\frac{1 - e^{-z/L(\theta)}}{1 + \left(\frac{\phi_M}{\phi_m} - 1\right)e^{-z/L(\theta)}} \right)^{\frac{3}{2}}. \quad (12)$$

With $\phi_m = 0.5$ and $\phi_M = 0.65$ the total flux flowing down the heap is

$$\frac{Q_{heap}}{D\sqrt{gD}} = 1.4 \frac{F_0^{5/2}}{\mu_{T0}^{1/2}} \frac{(\sin(\theta) - \mu \cos(\theta))^{1/2}}{\left(1 - \frac{\mu_N}{\mu_T}(\tan(\theta) - \mu)\right)^{5/2}}.$$

The dependence on θ of L and Q_{heap} are represented in Fig. 4, with $\mu = 0.36$ and $\mu_N/\mu_T = 4.7$.

2.2 Chute on rough plates

The flows over inclined rough plates are more difficult to handle because the constitutive equations (2) and (3) hold only in the bulk of the dense granular medium and are likely to be modified close to the rough plate. Since the role of the plate rugosity is difficult to assess quantitatively, we discard the description of the "basal layer" close to the plate [6, 8] and assume a slip velocity V_s at some distance δ above the rough plate. Then we apply (2) and (3) to a layer of thickness h , so that the free surface is located at a distance $h + \delta$ above the rough incline. In the slab of thickness h , the solid fraction increases from ϕ_m at the free surface to the value $\phi_{heap}(h)$ at a distance δ from the rough plate where the velocity is V_s . The total flux through the core region is now given by:

$$\begin{aligned} \frac{Q_{plate}}{D\sqrt{gD}} &= \frac{F(\phi_{heap}(h))}{1 - \frac{\mu_N}{\mu_T}(\tan(\theta) - \mu)} \frac{V_s}{\sqrt{gD}} + \\ &+ \frac{(\sin(\theta) - \mu\cos(\theta))^{1/2}}{\left(1 - \frac{\mu_N}{\mu_T}(\tan(\theta) - \mu)\right)^{5/2}} \int_{\phi_m}^{\phi_{heap}(h)} \left(\frac{F^3}{\mu_T}\right)^{1/2} \frac{\partial F}{\partial \phi} \frac{d\phi}{\phi}. \end{aligned} \quad (13)$$

A rough plate is likely to slow down the core region more efficiently than a heap would do and we expect $V_s \leq V_{heap}(h)$. As a consequence, $Q_{plate}(h, \theta)$ as given in (13) is not expected to exceed $Q_{heap}(\theta)$ given in (6). When forcing a flux Q_{plate} to flow down a rough plane inclined at angle θ , two different situations are encountered: when Q_{plate} is larger than $Q_{heap}(\theta)$, the granular medium will rearrange so as to flow down over a heap of angle $\theta + \alpha$ with $Q_{plate} = Q_{heap}(\theta + \alpha)$. This gives a possible explanation for the "immature sliding flows" that were observed in some experiments [3, 4]. Due to the very large increase of Q_{heap} with θ (see figure (4)) and because the experimental flux is limited to some maximal value, immature sliding flows were observed for small angles close to θ_{min} only. Conversely, when Q_{plate} is smaller than $Q_{heap}(\theta)$ the whole layer of thickness h is in motion with a velocity everywhere larger than V_s . Moreover, when $h/L(\theta) \lesssim 0.2$, the Bagnold-like velocity profile (which could hardly be observed in heap flows, see fig. (3)) is now invading the whole core region. In fact, when expressions (9) are taken for granted and $h/L(\theta) \lesssim 0.2$, the total flux (13) has the special form

$$\frac{Q_{plate}}{D\sqrt{gD}} = \frac{\phi_m V_s h}{D\sqrt{gD}} + \frac{2}{5} \phi_m^{3/2} \left(\frac{(\sin(\theta) - \mu\cos(\theta))}{\mu_{T0}} \right)^{1/2} \left(\frac{h}{D} \right)^{5/2}. \quad (14)$$

When the role of the velocity slip can be neglected, the second contribution gives the $h^{5/2}$ scaling which seems to be corroborated by experiments [14], as well as numerical simulations [15].

3 Confined shear flow

In the two-dimensional shear flows we will consider the pressure load exerted on the boundaries of the granular medium is supposed to be applied along direction z , which is thus the direction of main compression. Because gravity plays a minor role concerning the compressive forces, the constitutive relation for τ_{zz} is simply (compare with (2))

$$\tau_{zz} = \rho D^2 \mu_N(\phi) \left(\frac{dV}{dz} \right)^2 + \rho g DF(\phi), \quad (15)$$

whatever the angle θ between the z axis and gravity. The flow is along the x axis and the constitutive relation for the shear stress τ_{xz} is still given by (3), without any change as compared to the free-surface case.

3.1 Plane shear flow

As a first type of confined shear flow, we consider the planar shear of an infinite horizontal granular layer bounded by two plates separated by a fixed distance h . The pressure load and the gravity are both oriented along the direction z and the flow is along direction x (see figure 5). The equations of motion result in a constant shear stress S and a variable normal stress:

$$\tau_{xz} = S \quad \text{and} \quad \tau_{zz}(z) = P(0) + \rho g \int_0^z \phi(\xi) d\xi$$

where $P(0)$ is the pressure load exerted on the upper plate $z = 0$ ($z = h$ stands for the lower plate). We will distinguish the situation without and with gravity, the first case corresponding to numerical simulations and the second one to experiments.

3.1.1 Without gravity

In this case the normal stress is also a constant P all over the granular layer and the constitutive equations (15) and (3) give:

$$\begin{aligned} \rho D^2 \mu_T(\phi) \left(\frac{\partial V}{\partial z} \right)^2 &= S - \mu(\phi) P \\ \rho D^2 \mu_N(\phi) \left(\frac{\partial V}{\partial z} \right)^2 &= P - \rho g DF(\phi) \end{aligned} \quad (16)$$

Depending on the sign of $S - \mu(\phi)P$, we will have a static or a moving medium. In the static case the pressure load is noted P_0 and the shear is

such that $S \leq \mu(\phi_0)P_0$ where ϕ_0 is the constant compaction of the medium related to the pressure load through $P_0 = \rho g D F(\phi_0)$. In the dynamic case, the compaction is still ϕ_0 (mass conservation) while the shear S is now larger than $\mu(\phi_0)P_0$. The velocity gradient is constant:

$$\rho D^2 \left(\frac{\partial V}{\partial z} \right)^2 = \frac{S - \mu(\phi_0)P_0}{\mu_T(\phi_0) + \mu(\phi_0)\mu_N(\phi_0)}$$

Due to dilatancy effects the pressure load exerted on the plates is necessarily larger than in the static case, following:

$$P(S) = P_0 + \frac{S - \mu(\phi_0)P_0}{\mu(\phi_0) + \mu_T(\phi_0)/\mu_N(\phi_0)}.$$

As a consequence the effective friction coefficient is a function ϕ_0 and P :

$$\frac{S}{P} = \mu(\phi_0) + \frac{\mu_T(\phi_0)}{\mu_N(\phi_0)} \left(1 - \frac{\rho g D}{P} F(\phi_0) \right).$$

3.1.2 With gravity

In this case the normal stress increases in the downward direction so that the constitutive equation (3) results in

$$\rho D^2 \mu_T(\phi) \left(\frac{\partial V}{\partial z} \right)^2 = S - \mu(\phi)P(0) - \mu(\phi)\rho g \int_0^z \phi(\xi) d\xi$$

It is then clear that the gravity-induced extra compaction possibly induces shear localization because the right-hand side can have a different sign in different parts of the flow. To simplify this issue we will now introduce the same assumptions we have previously used in the free-surface shear flows, namely that μ and μ_T/μ_N do not depend on ϕ while $F(\phi)$ and $\mu_T(\phi)$ are given by (9). We will first describe the static case before considering grain motions. Because the compaction on the upper plate is necessarily different in the static and the dynamic cases, we define $P_0(0)$ as the pressure load exerted on the upper plate when the granular medium is motionless and $\phi_0(z)$ as the static compaction profile. As long as $S \leq \mu P_0(0)$, the granular slab is motionless, the compaction $\phi_0(0)$ at the upper plate satisfies $P_0(0) = \rho g D F(\phi_0(0))$ and the compaction profile is:

$$\phi_0(z) = \frac{\phi_M}{1 + \left(\frac{\phi_M}{\phi_0(0)} - 1 \right) e^{-z/L_0}} \quad \text{with} \quad L_0 = \frac{F_0}{\phi_M} D$$

When the granular medium is flowing, the compaction profile $\phi(z)$ displays larger gradients and becomes

$$\phi(z) = \frac{\phi_M}{1 + \left(\frac{\phi_M}{\phi(0)} - 1\right) e^{-z/L}} \quad \text{with} \quad L = \frac{L_0}{1 + \mu \frac{\mu_N}{\mu_T}}$$

where $\phi(0)$ is the new compaction at the upper plate. Since mass conservation requires

$$\int_0^h [\phi(z) - \phi_0(z)] dz = 0,$$

it is clear that $L < L_0$ results in $\phi(0) < \phi_0(0)$ and $\phi(h) > \phi_0(h)$. The compaction of the moving medium is thus reduced at the upper plate as compared to its static value while it is enhanced at the lower plate.

The velocity profile is then deduced from the compaction profile

$$\left(1 + \mu \frac{\mu_N}{\mu_T}\right) \frac{D}{g} \left(\frac{\partial V}{\partial z}\right)^2 = \frac{S^* - \mu F(\phi)}{\mu_T(\phi)}$$

where S^* is the dimensionless shear $\frac{S}{\rho g D}$. Let us define the volume fraction ϕ^* such that $S^* = \mu F(\phi^*)$. It is clear that $\phi^* > \phi_0(0)$ because $S > \mu P_0(0)$. However the above equation implies that motion exists for compactions less than ϕ^* only. This condition leads to check the self-consistency relation $\phi(z) < \phi^*$ for $0 < z < h$. This condition is automatically satisfied in the upper part of the flow since $\phi(0) < \phi_0(0) < \phi^*$. But it may be not in the lower part, thus leading to a shear localization. This localization phenomenon is here depending on S^* and h/L . Fig (6) shows the compaction and velocity profiles for two different values of $\phi^*(S^*)$ investigating the two different situations depending whether localization occurs or not.

3.2 Vertical chute flows

A second type of confined shear flow is the chute between two vertical plates (see figure 7). The compaction is due to a pressure load P exerted on the two plates along direction z . The flow and the gravity are oriented along direction x . The equations of motion result in a constant normal stress and a variable shear stress, by contrast to the preceding case:

$$\tau_{zz} = P \quad \text{and} \quad \tau_{xz} = \rho g \int_0^z \phi(\xi) d\xi,$$

where $z = 0$ corresponds to the symmetry plane located between the two plates at which the shear stress vanishes. The constitutive relation (3) implies

$$\rho D^2 \mu_T(\phi) \left(\frac{\partial V}{\partial z} \right)^2 = \rho g \int_0^z \phi(\xi) d\xi - \mu(\phi) P.$$

Either the right-hand side is everywhere negative (due to a very high pressure load) and the medium is motionless or there is a central region of the flow in which the shear stress does not exceed μP and consequently where the strain rate vanishes. In this plug flow regime the solid fraction is a constant ϕ^* related to the pressure load as $P = \rho g D F(\phi^*)$. The thickness z^* of the plug flow depends on ϕ^* (hence on the pressure load)

$$\frac{z^*}{D} = \frac{\mu(\phi^*)}{\phi^*} F(\phi^*).$$

Close to the vertical plates, there is a shear layer where the velocity decrease to V_w dependent on the plate roughness. In this parietal shear layer, the constitutive equations (15) and (3) imply:

$$\left(\frac{D}{g} \right)^{1/2} \frac{\partial V}{\partial z} = - \left(\frac{F(\phi^*) - F(\phi)}{\mu_N(\phi)} \right)^{1/2} \quad (17)$$

and

$$D \frac{\partial \phi}{\partial z} = \frac{\phi}{\frac{\partial}{\partial \phi} \left[\left(\mu + \frac{\mu_T}{\mu_N} \right) F(\phi^*) - \frac{\mu_T}{\mu_N} F(\phi) \right]}. \quad (18)$$

To obtain more definite results we again consider the assumptions already made for gravity-driven and plane shear flows, namely that μ and μ_N/μ_T are independent of the solid fraction while $F(\phi)$ and $\mu_T(\phi)$ are given by (9). Then, the compaction profile in the shear layer $z^* < z < z_w$ is:

$$\phi(z) = \frac{\phi_M}{1 + \left(\frac{\phi_M}{\phi^*} - 1 \right) e^{\frac{z-z^*}{L^*}}} \quad (19)$$

where L^* is the typical shear layer thickness:

$$\frac{L^*}{D} = \frac{\mu_T F_0}{\mu_N \phi_M}.$$

For the flow to be dense up to the vertical plates, the wall compaction ϕ_w must be larger than ϕ_m and the shear layer thickness is

$$\frac{z_w - z^*}{L^*} = \text{Log} \left(\frac{\frac{\phi_M}{\phi_w} - 1}{\frac{\phi_M}{\phi^*} - 1} \right).$$

As a consequence, the distance $2z_w$ between the two plates is a function of ϕ^* (hence of P) and of ϕ_w (hence of the plate roughness). Concerning the velocity, it increases from a value V_w at the wall to a value V_{plug} in the central part. The computed relative velocity field is represented in Fig (8) together with the fit

$$\frac{V(z) - V_w}{V_{plug} - V_w} = 1 - \left(\frac{\phi^* - \phi(z)}{\phi^* - \phi_w} \right)^{3/2}. \quad (20)$$

4 Comparison with experimental and (or) numerical data

4.1 Plane shear flow

Neglecting the influence of gravity (as was done in most numerical simulations) our model leads to a uniform solid fraction and to a uniform velocity gradient, in conformity with results presented in figures 5b and 5c of [16] for the dense flow regime. When gravity is taken into account, a shear localization is possible, depending on the magnitude of the pressure load as well as on the thickness of the granular layer. Unfortunately, we are unaware of experimental or numerical data with which the predictions of Fig. (6) could be tested.

4.2 Vertical chute flow

The uniform solid fraction and the uniform velocity in the core region are correctly reproduced by the model. Concerning the sheared regions closed to the vertical boundaries, the relative velocity profile (20) and the compaction profile (19) are quite similar to results presented in fig. 7b and 7c of [16].

4.3 Heap flow

The solid fraction profile (10) and the velocity profile (12) are quite close to those represented in fig.9b and 9c of [16] and in fig.9a and 9b of [17]. In particular, the velocity profile displays a Bagnold-like profile very close to the free-surface ($z < 0.2L(\theta)$), a quasi-linear profile in the central part of the flow ($0.2 < z/L(\theta) < 2$) and finally an exponential tail for the deepest parts of the flow, observed in [18]. At variance with confined flows for which the shear was localized in boundary layers with thickness of the order of a few grain diameters, heap flows are characterized by a thickness $L(\theta)$ of a few grain diameters when θ is slightly larger than θ_{min} but which increases

to quite large values when θ is close to θ_{max} . A similar unlimited increase of the grain flux Q_{heap} is observed for θ close to θ_{max} , as seen in fig. 4. Such a behaviour is difficult to observe experimentally due to the limited values of Q_{heap} that can be achieved in usual laboratory devices. According to (6) and (11), our model predicts $L \sim (Q_{heap})^{2/5}$ when θ is not close to θ_{min} , a result slightly different from the scaling $L \sim (Q_{heap})^{1/2}$ suggested by fig.9j of [16].

4.4 Rough inclined planes

We explained the appearance of the so-called "immature sliding flows": they develop when the imposed flux Q_{plate} over a plate with inclination θ is larger than the flux $Q_{heap}(\theta)$ which would fall down a heap with the same slope. Since Q_{plate} is experimentally limited to some maximum value, immature flows are observed for θ close to θ_{min} only. When θ comes close to θ_{max} , the thickness h of the granular layer flowing over the rough incline is smaller than the thickness of the grain layer which would flow down a heap with similar slope. And when h is less than $0.2L(\theta)$, the Bagnold-like velocity profile is invading the whole flowing layer, with the $h^{5/2}$ scaling for the flux Q_{plate} as a direct consequence (provided the first contribution to (14) is negligible). The main drawback of our model is its inability to explain the quantity $h_{stop}(\theta)$ introduced by Pouliquen [15] and which was confirmed in numerical simulations [14]. The first reason is that we assumed the friction coefficient μ to be independent of the solid fraction. As a consequence θ_{min} is a constant and h_{stop} vanishes as soon as $\theta > \theta_{min}$. A second reason is the possible inadequacy of our model close to the rough incline. In this basal or frictional layer [6, 8], the particle rotation plays an important role, the grain stress tensor is possibly non-symmetric and the solid fraction has a perturbed profile. All these phenomena would require a specific modelling. In fact the explanation of $h_{stop}(\theta)$ proposed by Mills et al. [10] involves constitutive relations which are different close to the boundaries from those holding in the bulk.

4.5 Annular shear

This special kind of shear flow was not considered here because to describe it, we would need to give a constitutive equation for the τ_{xx} component of the granular stress, besides those for τ_{xz} and τ_{zz} . This will be done in future work.

5 Conclusion

We proposed a model for dense granular flows which considers the solid fraction as the main microstructural parameter. The granular stress is partitioned in a way similar to that proposed by Savage [13, 4]. One of the distinctive features is a completely explicit expression for the contact stress which involves a function $F(\phi)$ of the solid fraction. The solid fraction profile mainly depends on the compressibility $dF/d\phi$ while the velocity profile is bound to $F(\phi)/\mu_T(\phi)$ where $\mu_T(\phi)$ is somehow analogous to the effective viscosity used in the kinetic theory approach of dilute granular flows [7, 8]. In principle the complete model contains two more functions of the solid fraction ($\mu(\phi)$ and $\mu_N(\phi)$) but we strived to show that not so bad predictions could be obtained after assuming the friction coefficient μ and the dilatancy ratio μ_N/μ_T to be independent of the solid fraction. Obviously, these are simplifying assumptions which can be released and improved. We also checked that the tentative (and simple) expressions (9) for $F(\phi)$ and $\mu_T(\phi)$ led to sound predictions. Needless to say that these expressions also can be improved. The main drawback of constitutive equations (2) and (3) is their possible failure in a thin layer close to rough boundaries. Their main advantage is to contain all the ingredients necessary to interpret the shear-localization phenomenon, and to be able to explain the quite different velocity profiles appearing in the stationary shear flows of dense granular materials.

References

- [1] Azanza E., “Ecoulements granulaires bidimensionnels sur plan incliné”, Doctoral Thesis from Ecole Nationale des Ponts et Chaussées, (1998).
- [2] Rajchenbach J., “Dense, rapid flows of inelastic grains under gravity”, *Phys. Rev. Letters*, **90** 144302 (2003).
- [3] Ancey C., Coussot P. and Evesque P., “Examination of the possibility of a fluid mechanics treatment of dense granular flows”, *Mech. Cohesive-Frictional Mat.* **1**, 385-403 (1996).
- [4] Savage S.B., “Granular flows down rough inclines - review and extension”, in *Proc. of US-Japan Seminar on New Models and Constitutive Relations in the Mechanics of Granular Materials*, ed. by Jenkins J.T. and Satake M., Elsevier Science Publishers, Amsterdam, pp. 261-282 (1982).

- [5] Johnson P.C., Jackson R., “Frictional-collisional constitutive relations for granular materials, with application to plane shearing”, *J. Fluid Mech.* **176** 67-93 (1987).
- [6] Ancey C. and Evesque P., “Frictional-collisional regime for granular suspension flows down an inclined channel” *Phys. Rev E* **62**, 8349-8360 (2000).
- [7] Bocquet L., Losert W., Schalk D., Lubenski T.C. and Gollub J.P., “Granular shear flow dynamics and forces: Experiment and continuum theory”, *Phys. Rev. E* **65** 011307 (2002).
- [8] M.Y. Louge, “Model for dense granular flows down bumpy inclines”, *Phys Rev E* **67**, 061303 (2003).
- [9] Goodman M.A., Cowin S.C., “Two problems in the gravity flow of granular materials”, *J. Fluid Mech.* **45** 321-339 (1971).
- [10] Mills P., Loggia D. and Tixier M., “Model for a stationary dense granular flow along an inclined wall”, *Europhys. Lett.* **45** 733 (1999).
- [11] Aranson I.S., Tsimring L.S., “Continuum description of avalanches in granular media”, *Phys. Rev. E* **64** 020301 (2001).
- [12] Da Cruz F., Chevoir F., Roux J.-N., and Iordanoff I., “Macroscopic friction of dry granular materials”, in *Proceedings of the 30th Leeds-Lyon Symposium of Tribology*, Dalmaz D. et al. Editors (2003).
- [13] Savage S.B., “Analyses of slow high concentration flows on granular materials”, *J. Fluid Mech.* **377** 1-26 (1998).
- [14] Silbert L. E., Landry J. W. and Grest G. S., “Granular flow down a rough inclined plane: transition between thin and thick piles”, *Phys. Fluids* **15**, 1-10 (2003).
- [15] Pouliquen O., “Scaling laws in granular flows down rough inclined planes”, *Phys. Fluids* **11** (1999).
- [16] G.D.R. Midi, “On dense granular flows”, *Eur. Phys J E* (submitted to).
- [17] Rajchenbach J., “Granular flows”, *Advances in Physics* **49** 229-256 (2000).
- [18] T.S. Komatsu, S. Inagaki, N. Nakagawa and S. Nasuno, “Creep motion in a granular pile exhibiting steady surface flow”, *Phys. Rev. Lett.* **86**, 1757-1760 (2001).

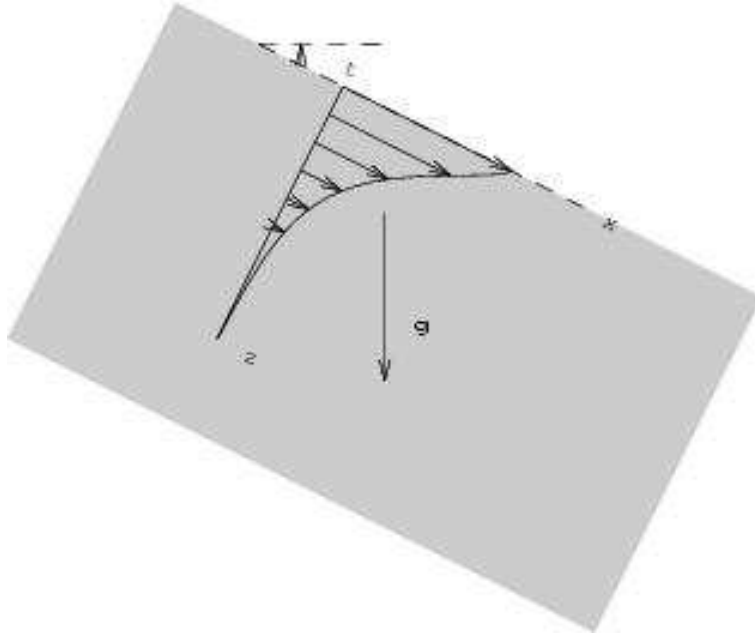


Figure 1: Gravity-induced shear flow with free surface (over a heap or an inclined plate with an angle θ relative to the horizontal plane).

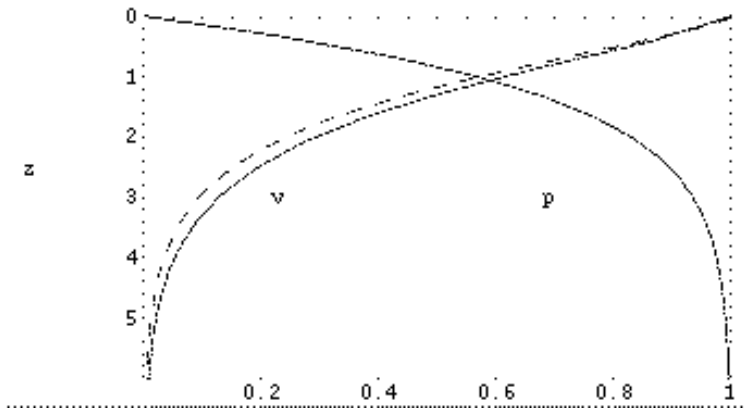


Figure 2: Reduced velocity profile $V_{heap}/V_{heap}(0)$ versus the adimensional distance $z/L(\theta)$ to the free surface. The dashed curve represents the approximate expression (12). The reduced compaction profile $(\phi - \phi_m)/(\phi_M - \phi_m)$ is plotted as well.

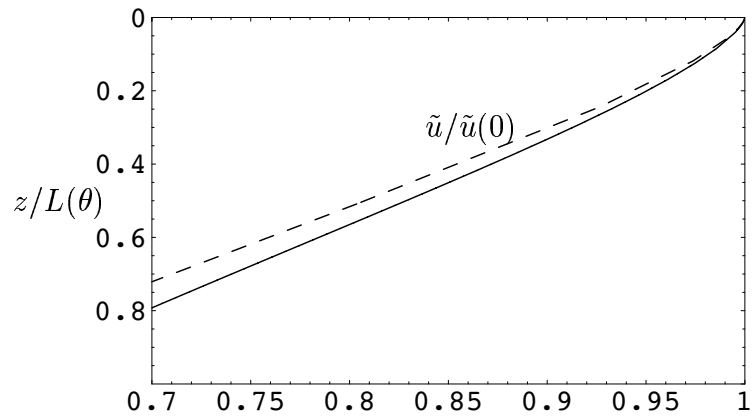


Figure 3: Zoom of figure 2 showing the Bagnold like region for $z/L(\theta) < 0.2$. The dashed curve represents approximation (12).

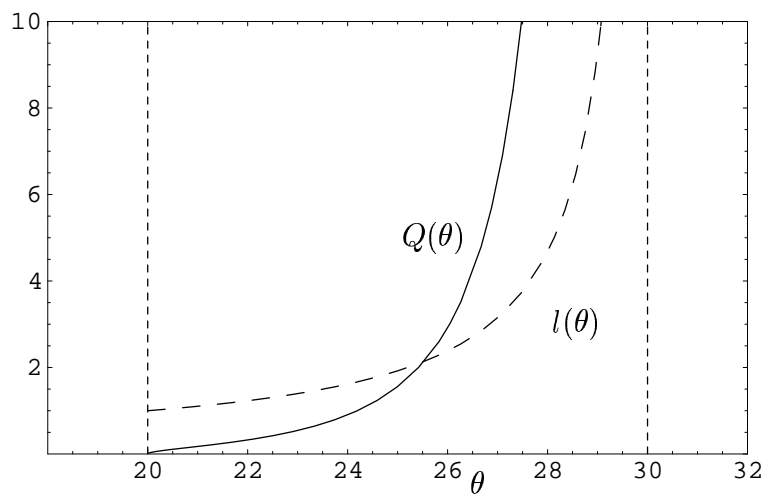


Figure 4: θ -dependance of flux Q_{heap} and adimensional thickness $l(\theta) = \phi_M L(\theta)/D$.

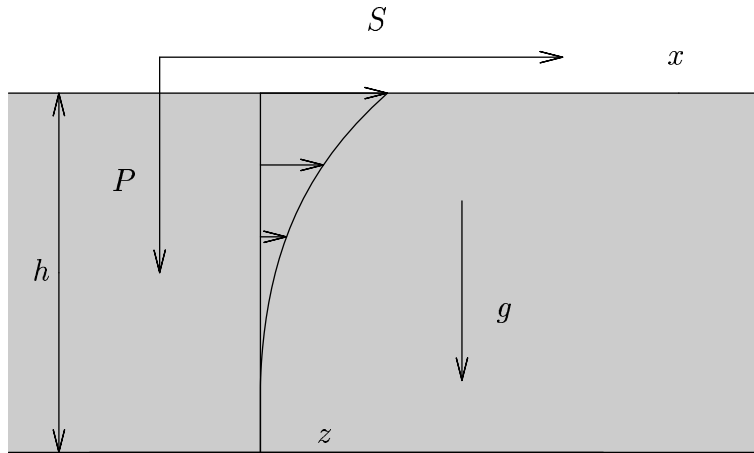


Figure 5: Planar confined shear flow of an infinite horizontal granular layer bounded by two plates separated by a fixed distance h . The pressure load P and the gravity are both oriented along the direction z , the shear stress S and the flow are along direction x).

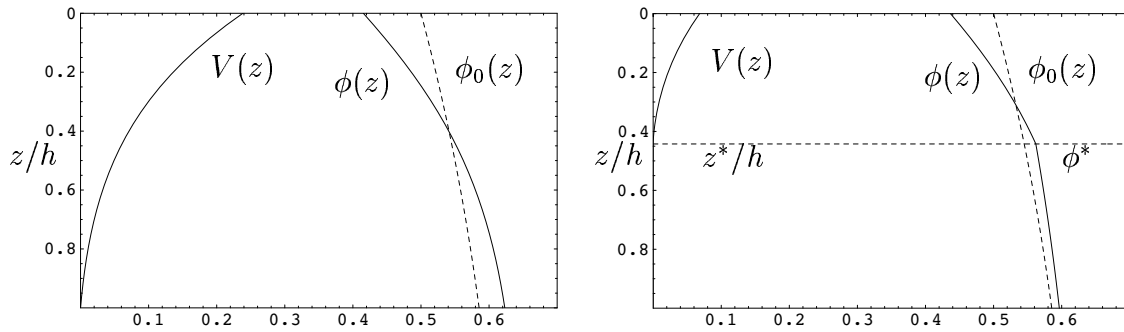


Figure 6: Velocity profile $V(z)$ and compaction profile $\phi(z)$, left large S , right small S .

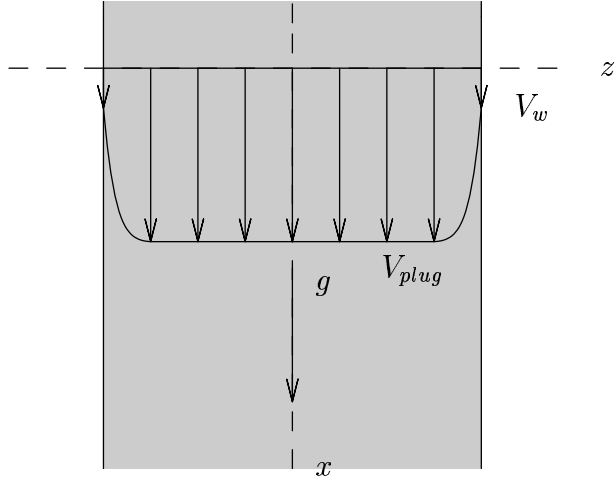


Figure 7: Vertical chute flow between two rough plates.

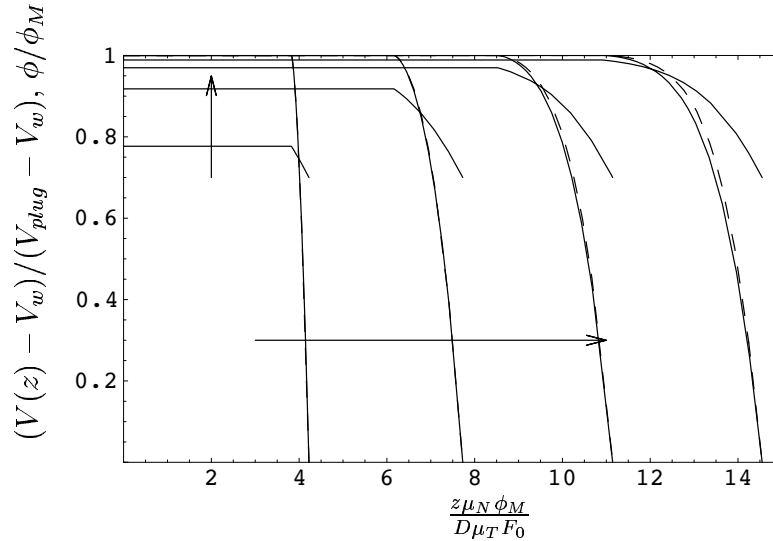


Figure 8: Reduced velocity profiles $(V(z) - V_w)/(V_{plug} - V_w)$ versus the adimensional distance $\frac{z\mu_N\phi_M}{D\mu_T F_0}$ to the center. The arrow is in the increasing values of $\frac{P}{\rho g D F_0}$. The dashed curve represents the approximate expression (20). The reduced compaction profiles ϕ/ϕ_M with $\phi_w/\phi_M = 0.7$ are plotted as well.